RASĀYAN *J. Chem.*
Vol. 19 | No. 3 | 1825-1833 | July-September | 2026
ISSN: 0974-1496 | e-ISSN: 0976-0083 | CODEN: RJCABP
http://www.rasayanjournal.com
http://www.rasayanjournal.co.in

COMPARATIVE EVALUATION OF SOL-GEL AND COPRECIPITATION SYNTHESIS OF Zr DOPED ZnO FOR ENHANCED SOLAR DRIVEN DEGRADATION OF P-NITROANILINE

N.P. Mali[1,✉], A. S. Bhosale[1], S. B. Dhotre[1], S. P. Takle[1], D. B. Bankar[2], R. U. Mene[3], and N. N. Bhujbal[1]

[1]Department of Chemistry, Annasaheb Magar Mahavidyalaya, Hadapsar-411028, Maharashtra, India

[2]Department of Chemistry, R. B. Narayanrao Borawake College, Shrirampur-413709, Maharashtra, India.

[3]Department of Physics, Annasaheb Magar Mahavidyalaya, Hadapsar-411028, Maharashtra, India

✉Corresponding author:malinetaji@gmail.com

ABSTRACT

This research highlights the success of zirconium (Zr) doping in ZnO matrix by comparing and applying cost-effective synthesis techniques like sol–gel (SG) and coprecipitation (CPPT) to enhance the electronic and surface properties of ZnO, thereby boosting solar-driven photocatalysis for industrial amine waste. The decline in band-gap energy to 2.88eV from 3.07eV along with an increase in oxygen vacancy concentration enhances visible-light absorption and decreases electron–hole recombination, leading to improved photocatalytic performance. The optimised Zr–ZnO nanocatalysts achieved around 74% degradation of p-nitroaniline and a significant decrease in TOC, indicating effective pollutant mineralisation. These findings provide valuable insights into the interplay between structure, properties and performance, emphasising the critical role of controlled dopant concentration (3–4 wt%) in balancing charge carrier dynamics and active site availability. Such understanding is crucial for the rational design of highly efficient photocatalysts. From an environmental perspective, this research contributes to Sustainable Development Goal-6 by presenting an effective method for eliminating toxic amine-based industrial pollutants using solar-assisted techniques. The synthesized material was analyzed by advanced techniques, including XRD, EDS, FE-SEM, UV-DRS, HR-TEM, Raman and XPS. In summary, this study advances environmental remediation technologies and lays the groundwork for future investigations into doped semiconductor systems for sustainable amine wastewater treatment using natural sunlight.

Keywords: Sol-Gel, Coprecipitation, Amine Degradation, ZnO, Zr-ZnO

RASĀYAN *J. Chem.*, Vol. 19, No. 3, 2026

INTRODUCTION

Increase in rapid urbanization and industrialization are frequently linked to increasing populations, both of which play a significant role in environmental mistreatment.[1] Harmful pollutants emitted by various manufacturing industries, agricultural runoff, household activities, pharmaceuticals, mining and marine oil spills can have a detrimental effect on aquatic life, endangering biodiversity and disturbing the fragile equilibrium of plant and animal life in the impacted regions.[2,3] Considering the widespread human use of amines and related substances, along with the potential danger of these chemicals entering water bodies, it is necessary to understand the concentrations, sources and mechanisms of amines in aquatic settings.[4] A recent work revealed that consuming polluted water has resulted in 3.20 million deaths globally.[5] Light-activated semiconductor photocatalysis was developed to enhance the degradation capabilities of previous methods, and it has been shown to fully break down wastewater.[6] Among the many inorganic photocatalysts recognized for their outstanding photocatalytic activity, zinc oxide has drawn a significant attention due to its unique characteristics like low cost, enhanced light-sensitivity, excellent physical as well as chemical stability, controlled morphology, easy synthesis, and environmental sustainability,

http://doi.org/10.31788/RJC.2026.1939746

making them excellent candidate for use in photocatalysis applications.[7] These nanoparticles are notable for their broad bandgap and high binding energy (60 meV), which endow them with remarkable electronic as well as optical features.[8] Zinc oxide nanoparticles are characterised by their robust activity of photocatalysis, high electron mobility & notable germicidal effectiveness, which makes them essential in a wide array of applications. The adaptability of zinc oxide nanomaterials is enhanced by the diverse synthesis routes available, including sol-gel,[9] hydrothermal,[10] chemical vapour deposition technique[11] and coprecipitation,[12] which allow for precisely tuned control on their surface properties. According to a literature review,[13] developed innovative nanoparticles showed high photocatalytic efficiency for degrading the amines such as aniline, p-nitroanilines etc under sunlight irradiation.[14,15] The integration of zirconium ions into the ZnO matrix, modification of the lattice, changes the electronic structure, leading to enhanced electrical and optical properties.[16] Incorporating zirconium has been depicted to increase band-gap energy and photocatalytic efficiency, making them suitable for UV and visible light-induced photocatalysis and also environmental cleanup.[17] Zinc oxide (ZnO) is well-known for its effectiveness as a photocatalyst, largely due to its affordability and eco-friendliness. However, its broad band gap and the rapid rate of recombination of electron–hole pairs greatly restrict its activity under visible light. Recent research indicates that doping with metals and rare-earth elements can significantly boost photocatalytic efficiency by lowering the band gap and creating defect states that enhance charge separation.[18–20] Despite this, there has been a lack of comprehensive studies on the combined effects of synthesis methods and optimised Zr doping on the solar-induced degradation of amine-based pollutants. Previous works with Zr-ZnO were focused on degradation of dyes,[19] disinfection byproducts,[20] organic carbonyl compounds[21] etc. Since, there were no previous work was done on the degradation of amine waste by using Zr-ZnO. This study seeks to examine Zr-doped ZnO produced through sol–gel and coprecipitation techniques with a focus on the relationships between structure, properties and performance for the effective degradation of p-nitroaniline. This research supports sustainable environmental cleanup efforts by creating cost-effective, solar-active photocatalysts for treating wastewater. Recent studies on Zr-doped ZnO nanoparticles have led to notable advancements in their preparation, characterisation, and practical uses.[22] The focus of the researchers has been towards refining the doping method to achieve consistent dispersion of Zr in the ZnO matrix, which is crucial for enhancing the properties of the nanomaterials. In this investigation, Zr-ZnO nanomaterials were prepared and thoroughly characterised to evaluate their morphological, structural and optical properties. p-Nitroaniline was used as an amine industrial waste to examine the photocatalytic performance of Zr-doped ZnO nanoparticles under sunlight exposure. These results underscore the adaptability of Zr-ZnO nanoparticles, demonstrating significant prospects in environmental cleanup, optoelectronics, and other advanced applications.

EXPERIMENITAL

Material and Methods

The synthesis process utilised zinc nitrate hexahydrate ($Zn(NO_3)_26H_2O$), zirconium oxychloride octahydrate ($ZrOCl_2$ $8H_2O$) and NaOH. All materials were analytical grade, sourced from Merck, & utilized as supplied. Throughout the synthesis, Millipore water with a conductivity of 0.06 μS/cm. *p*-Nitroaniline served as the pollutant for degradation performance testing.

Synthesis of Undoped Zinc Oxide and Zr-ZnO by SG and CPPT Synthesis

Zinc oxide nanomaterials were prepared using the sol–gel (SG) method by dissolving zinc nitrate hexahydrate at a concentration of 0.5M in water with continuous stirring at a temperature of 60°C. A 5% Sodium hydroxide (NaOH) solution was added drop by drop until the pH level reached approximately 8, which led to the formation of a gel. The gel was then aged with stirring for 12 hours, followed by drying below an infrared (IR) lamp and calcination at 700°C to yield ZnO powder. For Zr-doped ZnO, zirconium oxychloride was dissolved separately and mixed with the zinc precursor solution before gel formation. The same procedure was followed to obtain Zr–ZnO with varying dopant concentrations (1–5 wt%). In the coprecipitation method, NaOH was then added to the precursor mixture until pH ~12 to form a precipitate, which was then washed, dried and calcined under similar conditions.

Characterization

The X-ray diffraction (Rigaku Ultima IV, λ = 1.5406 Å, Cu Kα radiation) is used to analyse crystalline structure over a 2θ range of 20°–80°. Morphological analysis was carried out using FE-SEM (FEI Nova Nano SEM 450) and HR-TEM (Philips CM200) operating voltages ranging from 20kV to 200 kV, with 2.4 Å resolution. Elemental composition was determined using EDX (Bruker X-Flash 6I30). Optical properties were studied using a UV–Visible spectrophotometer (PerkinElmer), while Raman spectroscopy (HORIBA, 532 nm excitation) was used to examine vibrational characteristics.

RESULTS AND DISCUSSION

X-ray Diffraction Analysis (XRD)

The crystalline structure along with phase composition of the obtained nanoparticles were analysed using XRD, which is depicted in Fig.-1. The XRD pattern for zinc oxide and 1-5wt% of Zr-doped ZnO synthesised by SG (Fig.-1a) and CPPT (Fig.-1b) methods. It can be observed that all prepared material consists of polycrystalline grains within a hexagonal wurtzite phase. No additional impurity phases were observed in the ZnO nanocatalysts. The extinction of peaks related to Zr and ZrO_2 in the XRD pattern

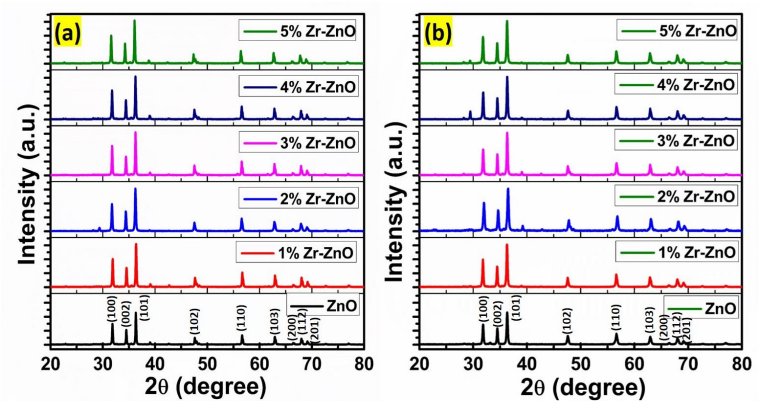

Fig.-1: X-Ray Diffraction Graph for ZnO and 1-5% Zr-ZnO for (a) Sol-Gel (b)Coprecipitation Method

indicates undoped ZnO formation. After doping with 1-5wt% Zr, The XRD revealed a strong bearing in the (101) plane, while the (100) and (002) planes were less prominent. Conversely, the (101) peak becomes highly pronounced when the Zr doping concentration is elevated to 5% by weight. The shifting of diffraction peaks toward lower 2θ angles in the doped samples indicates lattice expansion, which can be attributed to the replacement of Zn^{2+} ions having a size of 0.74 Å by larger Zr^{4+} ions (0.84 Å).[23] The Debye–Scherrer equation is implemented to calculate the crystallite size of the nanoparticles.[24]

$$D = \frac{0.9k}{\beta cos\theta}$$

In this equation, the incoming X-ray wavelength is denoted by k. FWHM is denoted by β, and the Bragg angle is denoted by θ. The average crystallite size and FWHM for synthesised Zr-ZnO (1wt%-5wt%) are 37.12 nm and 0.286, respectively, for SG. 3% Zr-ZnO shows a larger crystallite size of 33.47 nm. For CPPT, these values are 39.19 nm, and FWHM is 0.230 and 3% Zr-ZnO shows a larger crystallite size of 45.02 nm. The structural integrity and phase purity revealed by XRD play a crucial role in enhancing photocatalytic activity, thereby contributing to sustainable water purification strategies.

FESEM and TEM Analysis

The micro-structural characteristics of both undoped and Zr-modified ZnO nanomaterials were examined using FE-SEM and HR-TEM methods. Figure-2(a–d) presents SEM images that display nanoparticles with a predominantly hexagonal shape, distributed uniformly. The introduction of Zr results in noticeable particle clumping and a decrease in the average grain size, aligning with XRD findings and likely due to

the grain boundary pinning effect of Zr ions.[25] HR-TEM images (Fig.-2(e–f)) of 3 wt% Zr–ZnO, produced through sol–gel and coprecipitation techniques, demonstrate well-defined crystalline structures

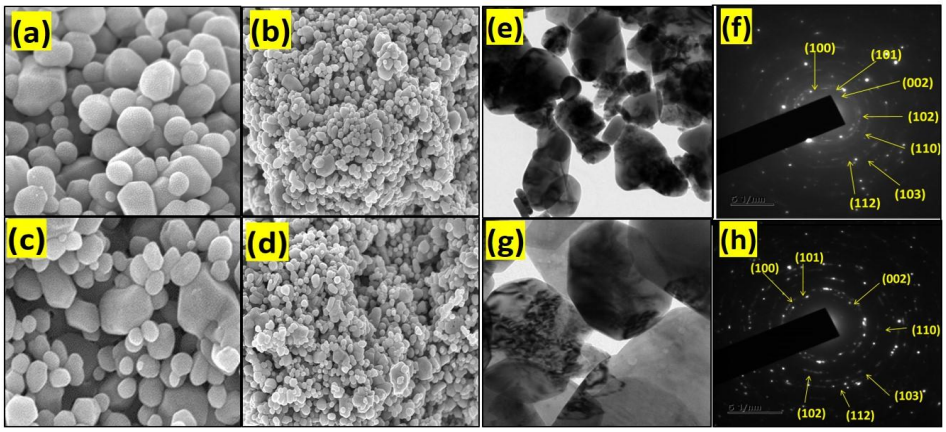

Fig.-2: SEM Images of Undoped ZnO (a & c), 3% Zr-ZnO by SG(b) and CPPT(d) Method. HR-TEM Images of 3% Zr Doped ZnO for SG(e) and CPPT(g) method. SEAD Pattern of 3% Zr-ZnO by SG (f) and CPPT(h) Method

with hexagonal and occasionally spherical shapes. The corresponding SAED patterns (Fig.-2(g–h)) reveal the polycrystalline nature of the doped ZnO, having distinct diffraction rings analogous to the wurtzite structure for both methods. EDAX analysis verifies Zn and O presence in undoped ZnO and Zn, O and Zr in the doped samples with no detectable impurities. Lattice fringe analysis indicates a d-spacing of 0.237 nm for the (002) plane. 0.273 nm for the (100) plane. The observed increase in interplanar spacing is attributed to lattice distortion caused by the substitution of larger Zr^{4+} ions in place of Zn^{2+}, resulting in slight expansion of the ZnO wurtzite lattice.

XPS Analysis

The oxidation states and dispersion of elements in the prepared nanomaterials were studied by using XPS (Fig.-3). Survey spectra (Fig.-3a) display diffraction peaks associated with the constituent elements, such as Zn, O, and Zr, which were identified, indicating the nanomaterial is free from impurities. The peaks with binding energies of 1022 eV and 1045 eV for Zn $2p_{3/2}$ and Zn $2p_{1/2}$, respectively, were observed (Fig.-3c) due to spin-orbit, which can be attributed to Zn^{2+} bonded with oxygen ions. Further, two prominent peaks are clearly visible and align with the reported values for Zn^{2+}.

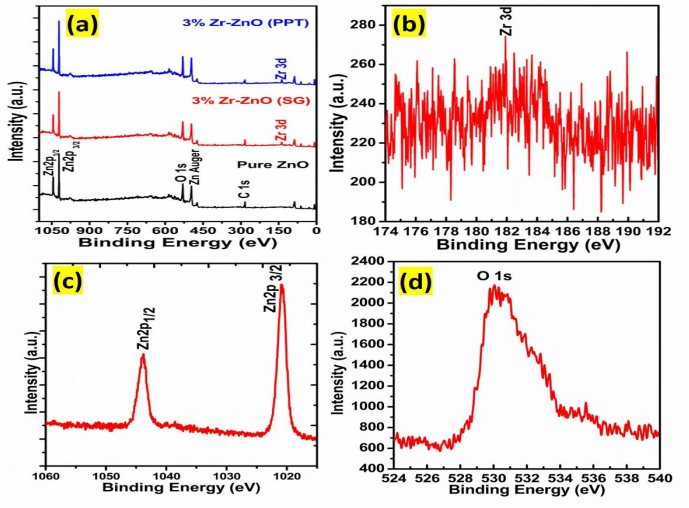

Fig.-3: XPS Spectrum of 3wt% Zr-ZnO (a) Survey Scan, (b) Zr 3d, (c) Zn 2p, (d) O 1s Spectrum for SG and CPPT Method

Figure-3(d) is the XPS analysis for O1S of 3% Zr doped ZnO, which displays an asymmetric profile consisting of two distinct components: a weak peak at 531.11 eV, a dominant peak at 529.52 eV. The former is associated with photoemission in O^{2-} ions that resemble valence oxygen adsorbed on the surface, O1s.[26] Consequently, the O1S peak for 3% Zr-ZnO appears asymmetric, with the 531.11 eV component being more prominent than in undoped ZnO, indicating a higher number of oxygen vacancies in 3% Zr doped ZnO. The high-resolution XPS scan of the Zr3d region reveals a notable peak. At 182 eV (Fig.-3b), assigned to the $3d_{5/2}$ state of Zr^{4+} ions[27] and peaks at 903.76, 907.2 and 916.3eV, assigned 23 eV binding related to Zn 2p spectrum of spin-orbit splitting was detected, aligning with reported values of Zn^{2+} in ZnO.[28,29]

UV-DRS Study

The optical absorption characteristics of the undoped and 3 wt% Zr-ZnO nanoparticles were investigated using UV–Visible spectroscopy. The Kubelka–Munk approach was applied to estimate the tauc plot of prepared nanocatalysts.[30] Insertion of Zr into the ZnO lattice leads to significant changes in the band gap energy. The decline in band gap from 3.07 to 2.98 eV for SG (Fig.-4a) & to 2.88 eV for the CPPT method (Fig.-4b). which can be attributed to Zr-induced defect states and oxygen vacancies.

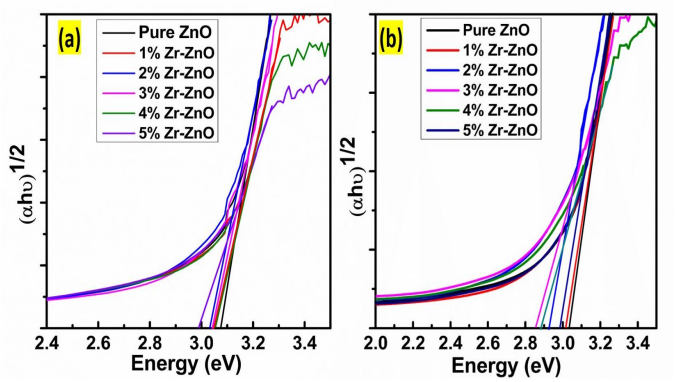

Fig.-4: Tauc plot for undoped ZnO and 1-5% Zr-ZnO through (a) Sol gel, (b) Coprecipitation method

This modification enhances visible-light absorption, thereby improving photocatalytic efficiency under solar irradiation. Other Zr-doped nanocatalysts show intermediate band gap values. This trend is consistent with earlier reports on doped ZnO systems, where band gap narrowing improves visible-light utilization. Thus, Zr doping suggests an efficient approach to modify the optical characteristics of zinc oxide for improved photocatalytic practices for the degradation of amine industrial waste.

Raman Spectroscopy

The Raman spectroscopy was utilized to evaluate the quality of crystals, structural imperfections and vibrational modes in the nanocatalyst. Figure-5 depicts the Raman spectroscopic profile of undoped ZnO

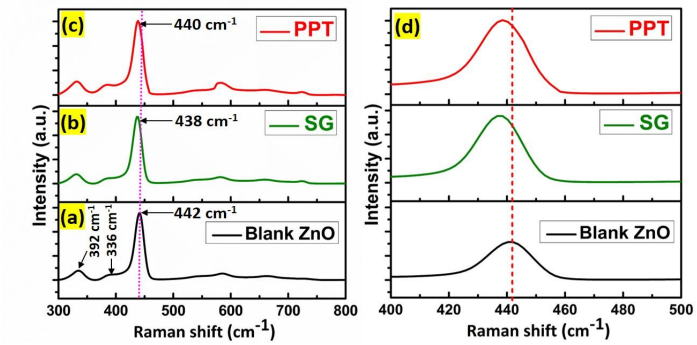

Fig.-5: Raman spectrum for (a) undoped ZnO. 3% Zr-ZnO by (b) SG, (c) CPPT method, (d) Raman shift for doped and undoped ZnO for SG and CPPT method

and 3%Zr doped ZnO.These spectra reveal various modes of vibration at 336 cm^{-1},392cm^{-1} and 442cm^{-1}.[36] A sharp and dominant peak was detected at 442 $cm^{-1,}$ identified as the E_2^{high} mode, indicating the distinctive electronic signature associated with the hexagonal wurtzite phase of ZnO powder. Detailed analysis reveals that the introduction of Zr^{4+} ions affects the vibrational characteristics and crystallographic structure of the zinc oxide nanocatalysts.[24] The inclusion of the Zr decreases the peak intensity to approximately 438 cm^{-1} and 440 cm^{-1} for the sol gel and CPPT methods, respectively. Also, the peak shifting is observed from 442 cm^{-1} for undoped ZnO to 438 cm^{-1} and 440 cm^{-1} for SG and CPPT, respectively. This shifting might result from the substitution of some Zn^{2+} atoms with Zr^{4+} in the ZnO lattice structure.

Photocatalytic Degradation of *p*-Nitroaniline

p-Nitroaniline is a yellow colored crystalline solid having molecular formula $C_6H_6N_2O_2$ and produces a pale to dark yellow color when dissolved in water. *p*-Nitroaniline is known for its strong UV-Vis absorption peak in the ultraviolet range, typically observed around 378-381 nm when dissolved in water.[31] This peak is associated with the $\pi \rightarrow \pi^*$ transition within its conjugated system. The photodegradation experiment was conducted using 30 ppm solutions of *p*-nitroaniline with 0.050 g of the nanocatalyst exposed to visible or sunlight during October from 11 am to 4 pm for a total of 360 minutes (6 hours). Under clear skies, the intensity of light was measured at 1100 using a Lux meter. The catalysts and p-nitroaniline solution were kept in darkness for 45 minutes before sunlight exposure to reach adsorption–desorption equilibrium. The experiments were conducted without a catalyst (As such) and with undoped ZnO, as well as with 1-5% Zr-ZnO synthesized through sol gel and coprecipitation methods. All Zr-doped ZnO samples showed good performance, but the 3% Zr-ZnO from the SG method and the 4% Zr-ZnO from the CPPT demonstrated better photocatalytic degradation compared to undoped ZnO alone, suggesting that adding Zr enhances ZnO's photocatalytic efficiency. However, increasing the Zr dopant concentration leads to reduced photocatalytic performance under the same conditions, likely because of ZnO's broad bandgap, theoretically 3.37 eV. 3.37 eV. The inability of visible light to initiate exciton formation leads to a reduction in photocatalytic efficiency. The elimination of p-nitroaniline when ZnO is present is due to the photosensitization of p-nitroaniline. An increased concentration of Zr obstructs active sites, thereby reducing photocatalytic activity. Figure-6 (a and b) for SG and (d and e) for CPPT illustrate the UV-Vis plot for the degradation of p-nitroaniline, while (c and f) depict the percentage degradation for the sole gel and CPPT method, respectively. Table-1 offers a comparison of the sol-gel and coprecipitation methods regarding the photocatalytic percentage degradation of p-nitroaniline, calculated using the relation,

$$\% \text{ Degradation} = [(A_0 - A_t)/A_0] \times 100$$

In this equation, A_0 denotes the initial concentration, while A_t denotes the final concentration of the *p*-nitroaniline. The comparative degradation of p-nitroaniline using the sol-gel and coprecipitation methods with varying levels of zirconium doping obeys pseudo-first order kinetics, which is in agreement with the Langmuir–Hinshelwood (L-H) model.

Table-1: The comparative degradation of p-nitroaniline using the sol-Gel and coprecipitation method with different concentrations of Zr

	% Degradation of *p*-nitroaniline					
Method	Undoped ZnO	1% Zr-ZnO	2% Zr-ZnO	3% Zr-ZnO	4% Zr-ZnO	5% Zr-ZnO
SG	13.29	18.38	21.10	73.61	50.34	39.46
CPPT	16.92	19.25	27.60	29.92	67.86	52.96

The photocatalytic degradation of *p*-nitroaniline effluent is checked for total organic carbon using the grab mode by the TOC analyzer. A lowering TOC suggests that the breakdown of *p*-nitroaniline converted into carbon dioxide, water, along with other gases and non-hazardous substances. Initially, the TOC of the sample before sunlight exposure was 16 ppm, and after photocatalytic degradation, it reduced to 2 ppm for 3% Zr-ZnO catalyst (SG method) and 3.5 ppm for 4% Zr-ZnO catalyst (CPPT method).

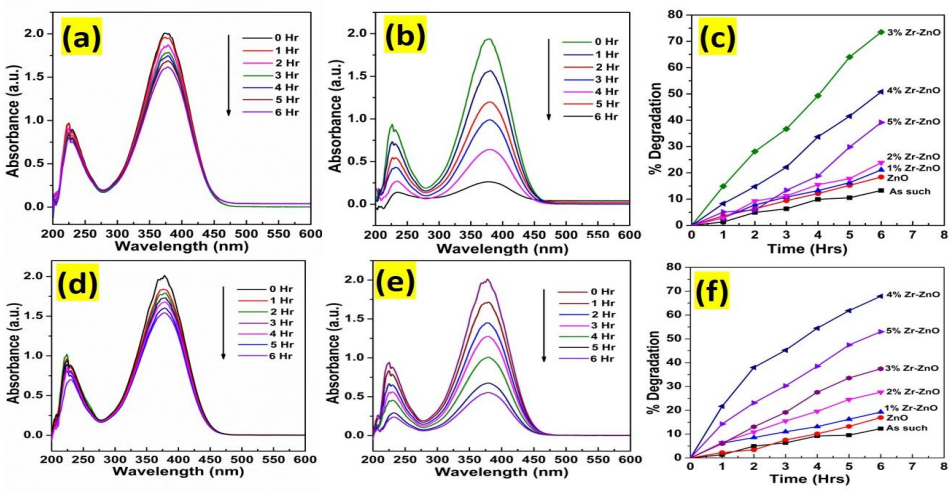

Fig.-6: UV-Visible spectra for degradation of p-nitroaniline (a)Undoped ZnO, (b)3% Zr-ZnO, (c) Total % degradation of 1-5% Zr-ZnO by SG method, and (d) Undoped ZnO, (e) 4% Zr-ZnO, (f) % degradation for 1-5% Zr-ZnO by CPPT method

This efficient degradation and mineralization of p-nitroaniline highlight the potential application of the developed catalyst in sustainable wastewater treatment. In the recycling study, the photocatalyst retains over 75% of its original activity for 3 cycles, after which the activity begins to gradually decline. This significant drop in performance may indicate catalyst inactivation because of poisoning at the surface, agglomeration or structural changes.

CONCLUSION

The study aimed to develop ZnO nano-catalysts by doping them with Zr at concentrations ranging from 1-5%, utilizing cost-effective and simple sol-gel and coprecipitation techniques. The results verified the successful integration of Zr^{4+} ions into the zinc oxide lattice. XRD analysis showed that the doped nanoparticles retained their hexagonal wurtzite structure. FESEM images revealed a morphological shift from spherical to hexagonal, with hexagonal shapes being predominant. HR-TEM displayed distinct lattice fringes, indicating high crystallinity. The reduction from 3.04 eV to 2.98 eV using the SG method and to 2.88 eV with the CPPT method. XPS analysis confirmed the effective incorporation of Zr4+ into the ZnO matrix, substituting Zn^{2+} with lattice oxygen as the main species, along with slight shifts in binding energy. The presence of oxygen vacancies was noted. In terms of photocatalytic performance, doping with Zr enhances the degradation rate of p-nitroaniline in visible light irradiation. The Zr-ZnO samples with 3% and 4% concentrations were particularly effective, achieving approximately 74% (SG) and 67% (CPPT) degradation of p-nitroaniline and reducing TOC by around 65-68% within 6 hours. The catalyst also showed good stability, maintaining over 75% of its activity after three consecutive reuse cycles without significant structural alterations. From a practical perspective, the use of simple and cost-effective synthesis methods combined with solar-driven operation shows the potential of Zr–ZnO as a sustainable material for wastewater treatment.

ACKNOWLEDGEMENTS

The author expresses heartfelt gratitude to Dr. Namdeo Bhujbal and Dr. Ravindra Mene for their invaluable guidance and unwavering support. Additionally, the author acknowledges Dr. Shrikant Takle and Dr. Digambar Bankar for engaging in insightful discussions. Appreciation is also extended to the Department of Chemistry at Annasaheb Magar Mahavidyalay, Hadapsar, Pune.

AUTHOR CONTRIBUTIONS

The present work is related to *SDG-6: Clean Water and Sanitation*. All the authors contributed significantly to this manuscript, participated in reviewing/editing and approved the final draft for publication. The research profile of the authors can be verified from their ORCID ids, given below:

N. P. Mali https://orcid.org/0009-0000-3018-8030

A. S. Bhosale https://orcid.org/0009-0007-1383-6383
S. B. Dhotre https://orcid.org/0009-0003-3026-5181
S. P. Takle https://orcid.org/0000-0003-2966-6175
D. B. Bankar https://orcid.org/0009-0004-5479-2450
R. U. Mene https://orcid.org/0000-0003-1248-4092
N. N. Bhujbal https://orcid.org/0009-0008-5778-1932

Cite this article as: N. P. Mali *et al.*, *Rasayan J. Chem.*, 19(3), 1825-1833(2026), https://doi.org/10.31788/RJC.2026.1939746

REFERENCES

1. H. Aziz, K. Hama, F. S. Mustafa, K. M. Omer, S. Hama, R. F. Hamara and K. O. Rahman, *RSC Advances*, **13**, 17595(2023), https://doi.org/10.1039/D3RA00723E.
2. X. Chen, H. Sun, O. A. Zelekew, J. Zhang, Y. Guo, A. Zeng, D. -H. Kuo and J. Lin, *Applied Surface Science*, **525**, 146531(2020), https://doi.org/10.1016/j.apsusc.2020.146531.
3. L. Liang, Z. Wang and J. Li, *Journal of Cleaner Production,* **237**, 117649(2019), https://doi.org/10.1016/j.jclepro.2019.117649.
4. A. N. Kumar, M. Balakrishna, U. Desai, R. Rakshith, K. M. Ambika, P. Soumya, C. R. Ravikumar, S. S. Vadivu and N. Naik, *Scientific Reports*, **15**, 338(2025), https://doi.org/10.1038/s41598-024-82764-2.
5. T. Münzel, O. Hahad, A. Daiber and P. J. Landrigan, *Cardiovascular Research*, **119**, 440(2023), https://doi.org/10.1093/cvr/cvac082.
6. C. Jaramillo-Páez, J. A. Navío, M. C. Hidalgo and M. Macías, *Catalysis Today*, **284**, 121(2017), https://doi.org/10.1016/j.cattod.2016.11.021.
7. W. Liu, R. Peng, X. Ye, J. Guo and L. Luo, *Applied Surface Science*, **560**, 150013(2021), https://doi.org/10.1016/j.apsusc.2021.01.118.
8. M. C. Uribe-López, M. C. Hidalgo-López, R. López-González, D. M. Frías-Márquez, G. Núñez-Nogueira, D. Hernández-Castillo and M. A. Alvarez-Lemus, *Journal of Photochemistry and Photobiology A: Chemistry*, **404**, 112866(2021), https://doi.org/10.1016/j.jphotochem.2020.112866.
9. H. Liu, J. Yang, Z. Hua, Y. Zhang, L. Yang, L. Xiao and Z. Xie, *Applied Surface Science*, **256**, 4162(2010), https://doi.org/10.1016/j.apsusc.2010.01.118.
10. N. R. Yogamalar and A. C. Bose, *Journal of Solid State Chemistry*, **184**, 12(2011), https://doi.org/10.1016/j.jssc.2010.10.024.
11. J. -M. Ntep, S. Hassani, A. Lusson, A. Tromson-Carli, D. Ballutaud, G. Didier and R. Triboulet, *Journal of Crystal Growth*, **207**, 30(1999), https://doi.org/10.1016/S0022-0248(99)00363-2.
12. T. Numpilai, N. Polsomboon, N. Dolsiririttigul, K. Jitapunkul, W. Donphai, T. Imyen, M. Chareonpanich and T. Witoon, *ACS Omega*, **10**, 20886(2025), https://doi.org/10.1021/acsomega.5c02289.
13. M. Pirsaheb, B. Shahmoradi, M. Beikmohammadi, E. Azizi, H. Hossini and G. Md Ashraf, *Scientific Reports,* **7**, 1473(2017), https://doi.org/10.1038/s41598-017-01461-5.
14. M. Montazerozohori, M. H.Habibi, S. Joohari and V. Khodadostan, *Annali di Chimica*, **97**, 1015(2007), https://doi.org/10.1002/adic.200790086.
15. C. Gouedard, D. Picq, F. Launay and P. -L. Carrette, *International Journal of Greenhouse Gas Control,* **10**, 244(2012), https://doi.org/10.1016/j.ijggc.2012.06.015.
16. M. A. Wahba, S. M. Yakout, W. A. A. Mohamed and H. R. Galal, *Materials Chemistry and Physics*, **256**, 123754(2020), https://doi.org/10.1016/j.matchemphys.2020.123754.
17. N. C. S. Selvam, J. J. Vijaya and L. J. Kennedy, *Industrial & Engineering Chemistry Research*, **51**, 16333(2012), https://doi.org/10.1021/ie3016945.

18. V. Anitha, K. Poonkodi, S. Jayabal, E. Elakkiya, P. Gowtham and S. Rajalakshmi, *Discover Chemistry*, **3**, 199 (2026), https://doi.org/10.1007/s44371-026-00652-2.
19. E. Cerrato, C. Gionco, I. Berruti, F. Sordello, P. Calza and M. C. Paganini, *Journal of Solid State Chemistry*, **264**, 42(2018), https://doi.org/10.1016/j.jssc.2018.05.001.
20. P. Singh, R. K. Singh and R. Kumar, *RSC Advances*, **1**1, 2512(2021), https://doi.org/10.1039/D0RA08670C.
21. P. Du, T. Su, X. Luo, X. Xie, Z. Qin and H. Ji, *Catalysts*, **9**, 716(2019), https://doi.org/10.3390/catal9090716.
22. Z. Muhammad, M. F. Amjad, H. Abbas, Z. Iqbal, A. Azhar, A. Yasin and H. Iesar, Proceedings of IEEE International Conference on Embedded and Ubiquitous Computing, pp.117–124(2021), https://doi.org/10.1109/EUC53437.2021.00025.
23. J. Zhang, D. Gao, G. Yang, J. Zhang, Z. Shi, Z. Zhang, Z. Zhu and D. Xue, *Nanoscale Research Letters*, **6**, 587(2011), https://doi.org/10.1186/1556-276X-6-587.
24. J. Ghosh, R. Ghosh and P. K. Giri, *Sensors and Actuators B: Chemical*, **25**4, 681(2018), https://doi.org/10.1016/j.snb.2017.07.110.
25. G. Murtaza, R. Ahmad, M. S. Rashid, M. Hassan, A. Hussnain, M. A. Khan, M. E. Ul Haq, M. Shafique and S. Riaz, *Current Applied Physics*, **14**, 176(2014), https://doi.org/10.1016/j.cap.2013.11.002.
26. M. D. Angelin, S. Rajkumar, J. P. Merlin, A. R. Xavier, M. Franklin and A. T. Ravichandran, *Ionics*, **26**, 5757(2020), https://doi.org/10.1007/s11581-020-03681-8.
27. S. R. Teeparthi, E. W. Awin and R. Kumar, *Scientific Reports*, **8**, 5541(2018), https://doi.org/10.1038/s41598-018-23648-0.
28. D. Zhu and Y. Shao, *International Journal of Electrochemical Science*, **13**, 3601(2018), https://doi.org/10.20964/2018.04.45.
29. G. Yuan, J. Xiang, H. Jin, L. Wu, Y. Jin and Y. Zhao, *Materials*, **11**, 96(2018), https://doi.org/10.3390/ma11010096.
30. M. Mahajan, S. Kumar, J. Gaur, S. Kaushal, J. Dalal, G. Singh, M. Misra and D. S. Ahlawat, *RSC Advances*, **15**, 2958(2025), https://doi.org/10.1039/D4RA08632E.
31. J. Lunagariya, A. Dhar and R. L. Vekariya, *RSC Advances*, **7**, 5412(2017), https://doi.org/10.1039/C6RA26722J.

[RJC-9746/2026]